# (Un)coupling the factors contributing to the interfacial activation of *Streptomyces rimosus* lipase: computational and spectrophotometric study

Mirsada Ćehić[a], Zlatko Brkljača[b, 1], Želimira Filić[a], Ivo Crnolatac[b], Dušica Vujaklija[a], Danijela Bakarić[b, *]

[a] Division for Physical Chemistry, Ruđer Bošković Institute, Bijenička 54, 10000 Zagreb, Croatia

[b] Division for Organic Chemistry and Biochemistry, Ruđer Bošković Institute, Bijenička 54, 10000 Zagreb, Croatia

*Corresponding author. E-mail: danijela.bakaric@irb.hr (Danijela Bakarić)

## Abstract

*Streptomyces rimosus* lipases (SrLip) present an enzyme class that catalyses the hydrolysis of triacylglycerols producing fatty acids and glycerols. The abrupt increase in catalytic activity of SrLip when found at water-oil interface is assigned as interfacial activation (IA). Since the latter is a complex function of interface charge, chemical composition, as well as substrate orientation and concentration, the role of individual factors and their combinations that trigger IA remains rather elusive. The aim of this work is to unravel the contribution of particular factor in IA by examining SrLip activity towards *p*-nitrophenylpalmitate (*p*-NPP) as a substrate incorporated in three chemically different self-assembled aggregates: gum Arabic, sodium deoxycholate and liposomes made of 1,2-dioleyl-*sn*-glycero-3-phosphocholine (DOPC) lipids, and at two different pH values (pH = 6.8 and pH = 10.0). Spectrophotometric (UV/Vis) study revealed that SrLip catalyses *p*-NPP hydrolysis when the substrate is embedded in sodium deoxycholate at both pH values, suggesting that the coupling of favorable interface charge and substrate orientation drives the interfacial activation. Moreover, especially in alkaline conditions (pH = 10.0), hydrolysis of the ester bond of the substrate incorporated in DOPC bilayers occurs when appropriate orientation, concentration and arrangement is accomplished. All experiments were conducted in

[1] Present address: Selvita d.o.o. Prilaz baruna Filipovića 29, 10000 Zagreb, Croatia.

parallel on an inactive mutant SrLipS10/A as a reference. The molecular-level details of particular interface and accompanied substrates examined by all-atom molecular dynamics simulations revealed that availability of *p*-NPP at these three interfaces decreases in the following order: sodium-deoxycholate > DOPC > model gum Arabic.

*Keywords*: *p*-nitrophenylpalmitate (*p*-NPP); *Streptomyces rimosus* lipase (SrLip); interfacial activation (IA); gum Arabic; sodium deoxycholate; 1,2-dioleyl-*sn*-glycero-3-phosphocholine (DOPC) liposomes.

## 1. Introduction

Long-chained triacylglycerides are natural substrates of lipases (triacylglycerol acylhydrolases, E.C. 3.1.1.3), enzymes ubiquitous in all kingdoms of life that catalyses hydrolysis of substrate ester linkage by decomposing it into fatty acids and glycerols [1–3]. Due to their diversity, hydrolytic properties and robustness microbial lipases represent important class of industrial biocatalysts [4–6] whose constant-growing global demand has intensified the search for new enzymes of similar performance and application [7]. The members of GDSL/SGNH lipolytic family [8] characterize five consensus sequence (blocks I-V) and four invariant catalytic residues: serine (S), glycine (G), asparagine (N), and histidine (H), found in blocks I, II, III and V, respectively. Spectrometric analysis of covalently-bound inhibitor to S10 (block I), located close to the N-terminus, revealed that this amino acid residue is essential for the activity of *Streptomyces rimosus* (SrLip, Q93MW7) [2,9–13] . With recently solved crystal structure [14], SrLip represent one of the best characterized member of GDSL/SGNH lipolytic family. The 3-D structure (PDB: 4HYQ) showed α/β/α fold typical for the SGNH superfamily, while molecular dynamics (MD) simulation and quantum-mechanical calculations suggested catalytic mechanism of SrLip based on use dyad (Ser 10 and His 216), instead of classical hydrolytic triads [14].

One of the SrLip unique features is interfacial activation [3,15–19], i.e the abrupt activity increase at water-oil interface which is supposed to originate from the opening of the lid, a flexible part of the lipase which enables access to its active site [2,20]. Although the mere existence of a water-oil interface is a necessary condition for interfacial activation to be possible at all, it is by no means sufficient for the latter to occur; in particular, the substrate must be available not only in terms of orientation but also in sufficient concentration, hydration must not exceed certain level and,

ultimately, fast and reversible penetration of hydrophobic residues of lipase precedes its conformational change that allows lid opening and substrate approach to the active site [17,21–23].

The activity of variously originated lipases is usually examined by their ability to hydrolyze alkylated *para*-nitrophenyl (*p*-NP) esters of different chain lengths. Unlike short-chain water-soluble *p*-NP derivatives that can exist as monomers, those with medium and long alkyl chains are insoluble in water and form aggregates of different sizes and shapes [24]. Therefore, the ability of SrLip to hydrolyze *para*-nitrophenol butirate (*p*-NPB) or palmitate (*p*-NPP) can only be tested by introducing emulsifiers into solutions. One of the most commonly used emulsifiers of long-chained triacylglycerides is gum Arabic. As a mixture of a highly branched polysaccharide complex with about 2% protein, its dissolution in water produces a low-viscosity solution that inhibits the coalescence of oil droplets [25–27]. Although raw gum Arabic is slightly acidic [26] (p$K_a$ is between 2.5 and 4.5 [28]), by changing the pH of the medium it is possible to (de)protonate numerous carboxylic groups and improve substrate emulsification, which has proven particularly successful when SrLip substrate is *p*-NPB [2]. Regarding SrLip activity towards *p*-NPP, the most appropriate emulsifier is found to be sodium deoxycholate (Na-deoxycholate) [29], a compound that makes supramolecular aggregates whose shapes and dimensions change depending on the pH value of the medium [30]. Since the two mentioned emulsifiers are most often used in the evaluation of the activity of different lipases, the influence of interfaces different from the previously mentioned ones on the latter are scarcely studied. For instance, in exploring the activity of *Thermomyces lanuginosa* Cajal *et al*. incorporated *p*-NPB into small (S) and large (L) unilamellar vesicles (UVs) constituted from lipid bilayers made of an anionic lipid 1-palmitoyl-2-oleoylglycero-*sn*-3-phosphoglycerol (POPG) and a zwitterionic one 1-palmitoyl-2-oleoylglycero-*sn*-3-phosphocholine (POPC) [31]. Although the mentioned lipase was found to bind to all interfaces, it adopts different conformation and, consequently, exert different catalytic activity: the lack of surface charge on both SUVs and LUVs made of POPC and the size of LUVs made of POPG prevented interfacial activation, whereas the conditions required for interfacial activation to happen are apparently met only on SUVs made from POPG [31]. However, Bohr *et al*. recently demonstrated that the activity of *Thermomyces Lanuginosus* towards triglicerides incorporated into liposomes made of 1,2-dioleyl-s*n*-glycero-3-phosphocholine (DOPC) with 8 % of 1,2-dioleyl-*sn*-glycero-3-phosphoserine (DOPS) (an anionic lipid) actually depends on the liposome curvature [32].

Overal, the interfacial activation remains an elusive complex function of an interface charge and composition, substrate size and concentration, as well as of their mutual interplay [21]. Since SrLip activity is difficult to predict when different surfaces and even slightly different substrates are used, it could be possible that separating the intertwined contributions of surface, substrate and surrounding medium could better characterize the concept of surface quality and thus shed light on the phenomenon of interfacial activation of SrLip. Therefore, in this work we studied the activity of a SrLip wild type towards *p*-NPP using UV/Vis spectroscopy when the latter is incorporated into three different interfaces: gum Arabic, Na-deoxycholate and liposomes made of DOPC. In DOPC bilayer different concentrations of *p*-NPP are incorporated in order to assess if the significant increase in *p*-NPP concentration might induce activation on, expectedly, inactive surface in terms of electrostatics, or the surface electrostatics and substrate are actually coupled factors. All self-assembled aggregates (*p*-NPP in gum Arabic, Na-deoxycholate and DOPC) are prepared in aqueous media of two different pH values (pH = 6.8 and 10.0) in order to characterize pH contribution to the lipase activity. These pH values were chosen since the stability of SrLip and its activity towards *p*-NPP was reported to be the highest at pH ~ 7 and at pH ~ 10, respectively [2]. In order to characterize every interface on a molecular level MD simulations of *p*-NPP incorporated into three different self-assembled aggregates are performed. Since in liposome suspensions several packing motifs of lipids (and fatty acids as the product of hydrolysis) can be found, DSC measurements are conducted on 1,2-dipalmitoyl-*sn*-glycero-3-phosphocholine (DPPC) in order to elucidate how the lipid (and fatty acid) arrangement changes with the change of *p*-NPP concentration and pH value of a medium. DPPC was taken instead of DOPC since in the instrumentally available temperature range (10−90 °C) it can go through different phases ($T_m \approx 41$ °C [33]) that provide insight into the packing of phosphatidylcholine lipids with and without a *p*-NPP, whereas it differs from DOPC only in the length of the hydrocarbon chains. Experiments analogous to those conducted on a SrLip (wild type) are performed on an inactive mutant with catalytic residue Ser10 to Ala (SrLipS10/A) as a control. Ultimately, using the results obtained in this work it might be possible to predict which factors, inherent to the particular interface, will prevail in the activation of the investigated lipase.

## 2. Experimental

### 2.1 Chemicals

Lipids 1,2-dioleyl-*sn*-glycero-3-phosphocholine (DOPC; white powder) and 1,2-dipalmitoyl-*sn*-glycero-3-phosphocholine (DPPC; white powder) were purchased from Avanti Polar Lipids (≥ 99 %). Gum Arabic (white powder, p. a.) and sodium deoxycholate (Na-deoxycholate; white powder, p. a. grade) were both supplied from Sigma Aldrich. *Para*-nitrophenylpalmitate (*p*-NPP; pale yellow powder) was purchased from Alfa Aesar (98 %). Phosphate buffer ($I$ = 10 mM) of pH 6.8 in milli-Q water was prepared from $Na_2HPO_4$ and $NaH_2PO_4$, both purchased from Kemika (p. a. grade). Carbonate-bicarbonate buffer ($I$ = 100 mM) of pH 10.0 in milli-Q water was prepared from $NaHCO_3$ (white powder) and $Na_2CO_3$ (white powder) supplied from, respectively, Gram-Mol (p. a. grade) and Kemika (p. a. grade). Sodium chloride (NaCl; white powder, Alkaloid, p. a. grade) was added in both buffers so the ionic strength was $I$(NaCl) = 200 mM. Chloroform ($CHCl_3$; colorless liquid) and ethanol (EtOH; colorless liquid) were purchased from Gram-Mol (p. a. grade). 1,4-Dioxane (dioxane; colorless liquid, p. a. grade) was supplied from Sigma Aldrich. All chemicals were used as received.

## 2.2 Samples preparations

### 2.2.1 Lipases

*Streptomyces rimosus* GDSL lipase wild type (SrLip) was produced in a heterologous host *Streptomyces lividans* TK23. Lipase gene, *srl* was subcloned from plasmid pDJ5 [9] into a bifunctional *E. coli*/*Streptomyces* vector pANT849pWB19N [34] using described protocols [29]. The resulting construct carried a six his-tag sequence at the 3'-end of *srl* gene [35]. Growth media and culture conditions were described following procedure developed in previous study [29] with slight modification. Cell biomass was removed by centrifugation (5000 x g 15 min) and proteins were precipitated from the culture supernatant by $(NH_4)_2SO_4$ (80%). After dialysis, lipase purification was performed using Ni-NTA agarose (QIAGEN, Germany) column in binding buffer (50 mM Tris–HCl pH 8.0, 300 mM NaCl). Unspecifically bound proteins were efficiently removed from the column using the same buffer supplemented with 30 mM imidazole (Sigma, USA) thus avoiding the need for additional gel-filtration. Completely inactive SrLip, due to the mutation of essential catalytic residue Ser10 to Ala (SrLipS10/A), was used as a negative control [35]. Mutated enzyme, SrLipS10/A was purified as described above. Eluted fractions were desalted on a PD10 column (Pharmacia) equilibrated with 20 mM phosphate buffer (pH 6.8) and 20 mM NaCl and analyzed by SDS-PAGE. Protein concentrations were determined using

NanoDrop 2000 (Thermo Fisher Scientific, USA). The stock solutions of obtained lipases were prepared by dissolving them in buffers of pH values of 6.8 and 10.0 so their concentrations were *c*(SrLip / SrLipS10/A) = 40 μM (0.01 mg / ml).

2.2.2 *p*-Nitrophenylpalmitate (*p*-NPP) in 1,4-dioxane (dioxane)

*p*-NPP (0.60 mg) was dissolved in dioxane to give a concentration of stock solution *c*(*p*-NPP) = 13.2 mM. The latter was further mixed with buffers (pH = 6.8 and 10.0) so that the total volume of a mixture was 5 ml making the final concentration of *p*-NPP in prepared solutions *c*(*p*-NPP) = 0.32 mM and the mass fraction of dioxane ω = 2.5 % [35]. The solution thus prepared was sonicated for 2 minutes [29], left standing for 5 minutes [35] and used in further experiments.

2.2.3 Suspensions

2.2.3.1 Aggregates of gum Arabic. In 5 ml of the solution of *p*-NPP (*c*(*p*-NPP) = 0.32 mM) in a mixture of particular buffer and dioxane (ω = 2.5 %) (prepared in 2.3 subsection) gum Arabic was added (0.05 g) so that mass fraction of gum Arabic was ω = 1 %.

2.2.3.2 Aggregates of sodium deoxycholate (Na-deoxycholate). The aggregates of Na-deoxycholates with incorporated *p*-NPP were prepared analogously to the procedure described in 2.2.3.1 (Aggregates of gum Arabic) with the exception that Na-deoxycholate (0.01 g) was added instead of gum Arabic thus giving its mass fraction of ω = 1 % (*c*(Na-deoxycholate) = 5 mM).

2.2.3.3 Liposomes. Stock solutions of lipids (DOPC and DPPC) and *p*-NPP in $CHCl_3$ (colorless solutions) were prepared as follows: 65 mg of DOPC, 60 mg of DPPC and 4 mg of *p*-NPP were dissolved in 10 ml, 1 ml and 10 ml of $CHCl_3$, respectively. Their final concentrations in stock solutions were *c*(DOPC) = 8.7 mM, *c*(DPPC) = 81.7 mM and *c*(*p*-NPP) = 1.1 mM. The prepared solutions were used for making two sets of suspensions in two different buffers: pH 6.8 (phosphate buffer) and pH 10.0 (carbonate-bicarbonate buffer). Further, suspensions of DOPC were used for UV/Vis measurements and those of DPPC for DSC measurements in order to determine the existence of phase separation in the presence of *p*-NPP. Mixtures of DOPC and *p*-NPP at mole ratios *x*(*p*-NPP) of 2 % and 20 % were made by pipetting 1 ml of stock solution of DOPC and, respectively, 145 μl (for *x*(*p*-NPP) = 2 %) and 1909 μl (for *x*(*p*-NPP) = 20 %) of stock solution of *p*-NPP in a round bottom flask (*x*(*p*-NPP) = 2 % and 20 % corresponds to *ω*(*p*-

NPP) = 0.9 % and 10.5 %, respectively). One flask with only 1 ml of DOPC stock solution ($x/\omega$(*p*-NPP) = 0 %) was used as a reference. Mixtures of DPPC and *p*-NPP at the same mole ratios were made by pipetting 333 μl of DPPC stock solution (20 mg) and, respectively, 500 μl (for $x$(*p*-NPP) = 2 %) and 6.5 ml (for $x$(*p*-NPP) = 20 %) of stock solution of *p*-NPP in round bottom flasks. One flask with only 333 μl of DPPC stock solution ($x$(*p*-NPP) = 0 %) was used as a reference. In all twelve mixtures (6 x 2) $CHCl_3$ was removed from the flask on rotary evaporator and the obtained film was subsequently dried under Ar stream.

Following the solvent evaporation, multilamellar DOPC and DPPC liposome suspensions were prepared by Bangham's method [36]. Briefly, DOPC films were suspended in 10 ml, whereas DPPC films in 4 ml of either phosphate (pH 6.8) or carbonate-bicarbonate buffer (pH 10.0). The samples were vortexed and alternated between a hot $H_2O$ bath and a liquid $N_2$ bath. In each of these three steps the sample was held for about one minute. The cycle of vortexing and heating and cooling of the sample were repeated for five times. The final concentrations of DOPC and *p*-NPP in the suspensions were: $c$(DOPC) = 0.8 mM (6.5 mg / ml) for $x$(*p*-NPP) = 0 %, $c$(DOPC) = 0.8 mM (6.5 mg / ml) and $c$(*p*-NPP) = 1.6 nM (0.06 mg / ml) for $x$(*p*-NPP) = 2 % and $c$(*p*-NPP) = 20 nM (0.8 mg / ml) for $x$(*p*-NPP) = 20 %. Analogous quantities in suspensions of DPPC and *p*-NPP were $c$(DPPC) = 81.7 mM (5 mg / ml) and $c$(*p*-NPP) = 0.1 mM (0.05 mg / ml) for $x$(*p*-NPP) = 2 % and $c$(DPPC) = 81.7 mM (5 mg / ml) and $c$(*p*-NPP) = 1.7 mM (0.7 mg / ml) for $x$(*p*-NPP) = 20 %. Finally, dioxane was added to the suspensions of DOPC thus prepared so that its mass fraction ($\omega$) in the solution was 2.5 % as in other prepared suspensions (subsections 2.2.3.1 and 2.2.3.2).

Unilamellar liposomes of DOPC, both without (blank) and with incorporated *p*-NPP, were obtained by extrusion of prepared multilamellar suspension through 100 nm polycarbonate (Whatman) membrane at room temperature at least 31 times. Their size distribution of was determined by means of dynamic light scattering using a photon correlation spectrophotometer equipped with a 532 nm (green) laser (Zetasizer Nano ZS, Malvern Instruments, Worcestershire, UK). To avoid overestimation arising from the scattering of larger particles, the average hydrodynamic diameter (dh) was obtained as the value at peak maximum of the volume size distribution. The reported results correspond to the average of six measurements at 25 °C. The data processing was done by the Zetasizer software 7.13 (Malvern Instruments). The prepared

suspensions (0.5 mg / 10 ml) contain liposomes with hydrodynamic diameter ($d_h$) in the range $d_h \approx$ 100-200 nm (for details on DLS measurements see Supporting Information, section S1).

All samples (subsections 2.2.2 and 2.2.3) are further treated with lipases immediately after their preparation. The procedure was as follows: in a cuvette (total volume of $V$ = 1 ml) was added 990 μl of a solution prepared in 2.2.2 and suspensions prepared in 2.2.3 subsections. In this solution and suspensions made in 2.2.3.1 and 2.2.3.2 the concentration of lipase was $c$(SrLip / SrLipS10/A) = 0.4 μM and the concentration of *p*-NPP was $c$(*p*-NPP) = 0.32 μM; in liposomes made with $x$(*p*-NPP) = 0 %, 2% and 20 % ($c$(*p*-NPP) = 0 nM, 1.6 nM and 20 nM; $\omega$(*p*-NPP) = 0 %, 0.9 % and 10.5 %) the final concentrations of lipases were $c$(SrLip / SrLipS10/A) = 2 nM, 2 nM and 27 nM, respectively (2.2.3.3). All these systems were incubated for 1 min before starting UV/Vis measurements at room temperature.

2.3 UV/Vis spectroscopy: data acquisition and spectra analysis

UV/Vis spectra were measured on Agilent Cary 100 UV/Vis spectrophotometer in the cuvette of the pathlength $d$ = 1 cm in the spectral range 350-750 nm. Except for the dioxane, the spectrum of which was used as baseline and automatically subtracted from the suspension spectra (see Fig. S1 in Supporting Information), all samples were measured as duplicates. Obtained UV/Vis spectra were smoothed using Savitzky-Golay (SG) procedure and further analyzed in the spectral range 350-500 nm after one-point (at 500 nm) baseline correction using Spectragryph [37] (the comparison of raw and smoothed UV/Vis spectra is displayed in Fig. S2 in Supporting Information, and the average UV/Vis spectrum with the greatest uncertainty is displayed in Fig. S3, respectively). After this simple baseline correction, the spectra of *p*-NPP incorporated into gum Arabic / Na-deoxycholate / DOPC were subtracted from the corresponding spectra of *p*-NPP in gum Arabic / Na-deoxycholate / DOPC in the presence of SrLip / SrLipSer10/A, respectively (see Fig. 1). Due to the high noise level, the obtained difference spectra of *p*-NPP in the presence of SrLip / SrLipSer10/A obtained in gum Arabic at pH = 10.0 (Fig. 1b) were additionally smoothed (SG) and, along with analogous spectra obtained at pH = 10.0 in Na-deoxycholate, were baseline corrected (two end points).

2.4 DSC: measurements conditions and thermal analysis

DPPC suspensions (without and with *p*-NPP, as described in 2.2.3.3) were held for 15 minutes in a degassing station before they were placed in the cell and measured. The calorimetric measurements were carried out in a microcalorimeter Nano-DSC, TA Instruments (New Castle, USA) at a scan rate of 1 °C $min^{-1}$, temperature range 10-70 °C and cell volume of 300 μL. Data analysis was done using the TA Instruments Nano Analyze software package. All six suspensions (DPPC + 0 % *p*-NPP, DPPC + 2 % *p*-NPP, DPPC + 20 % *p*-NPP in buffers of pH = 6.8 and pH = 10.0) were recorded in two heating–cooling cycles as duplicates (DSC curve with the greatest uncertainty is displayed in Supporting Information, Fig, S4). The buffer-buffer (6.8–6.8 and 10.0–10.0) scans were collected once in two heating–cooling cycles (as suspensions) and subtracted from the corresponding raw suspensions data. The baseline was manually constructed and subtracted from the resultant curve. $T_p$ and $T_m$ of DPPC (as well as phase transition temperatures of other species aggregates) were determined from the maxima of thermal history-unburdened second heating run curve [38].

## 3. Molecular dynamics simulations

We performed all-atom molecular dynamics (MD) simulations of *p*-NPP in three different environments, namely in the model system mimicking gum Arabic/water mixture, Na-deoxycholate/water mixture and DOPC bilayer, with the three environments/systems being denoted as model gum Arabic, Na-deoxycholate and DOPC, respectively. The systems were prepared as follows: a) model gum Arabic system was built by introducing 6 *p*-NPP molecules into layer consisting of 50 branched glycan oligomers closely corresponding to the sequence shown in [39]. More precisely, the sequence corresponding to each glycan molecule is DGal+β1-3[LRha+α1-4DAra+β1-6DGal+β1-6]DGal+β1-3DGal+β1-3[LRha+α1-4DAra+β1-6DGal+β1-6]DGal+β1-3DGal+β1-3[LRha+α1-4DAra+β1-6DGal+β1-6]DGal+β1-3DGal+β1-OMe, with DGal, DAra and LRha corresponding to D-Galactose, D-Arabinofuranose and L-Rhamnose, respectively. Layer containing 50 model gum Arabic oligomers and 6 *p*-NPP molecules was immersed into 13200 water molecules, containing 49 sodium and 49 chloride ions ($I$ = 200 mM). b) Na-deoxycholate system was built by incorporating 13 *p*-NPP molecules into deoxycholate layer (≈ 8 nm thick) containing 250 Na-deoxycholate moieties with the deoxycholate layer being solvated using 13200 water molecules. Finally, c) DOPC system containing *p*-NPP was built by incorporating 13 *p*-NPP molecules into DOPC bilayer containing 128 DOPC lipids, with the

lipid being solvated by 5120 water molecules, and the ionic strength being again set at $I$ = 200 mM, corresponding to the experimental conditions (19 sodium and 19 chloride ions).

All aforementioned systems were built using Packmol package [40], with layers containing model gum Arabic/Na-deoxycholate/DOPC moieties together with *p*-NPP molecules built so that they initially reflect the expected density of the particular system at hand. All of the constituents of the three prepared systems were obtained using either AMBER of AMBER compatible force fields. More precisely, DOPC lipids are described using Slipids Force Field [41], which is compatible with AMBER force fields, *p*-NPP and deoxycholate moieties are described via general AMBER force field [42], model gum Arabic is parameterized using GLYCAM06 force field [43], while water molecules and salt ions were described by the standard TIP3P water model and via parameters developed by Joung and Cheatham, III [44] (ion parameters used in AMBER force fields), respectively.

Missing partial charges of *p*-NPP and deoxycholate moieties were estimated by a restrained single-conformer fit to the electrostatic potential (RESP) [45]. The potential was obtained from the HF/6-31G(d)//B3LYP/6-31G(d) quantum mechanical calculations in both cases.

All three prepared systems were subjected to the equivalent minimization/equilibration procedure. The simulation boxes were first minimized using steepest descent algorithm (5000 steps), and were subsequently relaxed for the duration of 1 ns at $T$ = 298.15 K (NVT ensemble) with the time step of 2 fs, where we used Berendsen thermostat (time constant for temperature coupling set at 1 ps), and where position restraints on all heavy atoms (all atoms other than hydrogens) were imposed (500 kJ $mol^{-1}$ $nm^{-2}$). After the initial relaxation in the canonical ensemble, systems were equilibrated at $T$ = 298.15 K (NPT ensemble), where we used Nosé-Hoover thermostat to maintain temperature (time constant for temperature coupling set at 1 ps) and Berendsen barostat to maintain constant pressure of 1 bar (time constant for pressure coupling set to 5.0 ps, semiisotropic conditions) for 10 ns with the time step of 2 fs with weak position restraints again applied on the equivalent set of atoms as aforementioned (100 kJ $mol^{-1}$ $nm^{-2}$). Finally, we propagated production runs, with all systems being simulated for 150 ns. Production simulations of all prepared systems were propagated in NPT ensemble without any restraints, with Nose-Hoover thermostat incorporated to maintain temperature at $T$ = 298.15 K (time constant for temperature coupling of 1 ps), whereas Parrinello-Rahman barostat was used

to maintain constant pressure of 1 bar (time constant for pressure coupling set to 5.0 ps, semiisotropic conditions). All simulations were performed with periodic boundary conditions in all three directions, with long-range electrostatic interactions beyond a 1.2 nm cutoff taken into account via the particle mesh Ewald method [46]. In the subsequent analysis only the last 50 ns of each individual simulation was considered. All MD simulations were conducted using GROMACS 2018 [47]. The systems are visualized by program VMD [48].

## 4. Results and discussion

The formation of the hydrolysis product is relatively easy to monitor using UV/Vis spectroscopy, as *p*-nitrophenol generally absorbs at about 350 nm, while *p*-nitrophenolate at about 400 nm [49–51]. Obtained subtracted spectra that display the signature of *p*-NPP in the presence of SrLip (solid lines) / SrLipSer10/A (short dashed lines) in gum Arabic (Figs. 1a) and 1b)), Na-deoxycholate (Figs. 1c) and 1d)) and in DOPC bilayers (Figs. 1e) and 1f)) reveal some important differences (unsubtracted spectra are displayed in Supporting Information, Fig. S5). In a phosphate buffer of pH value 6.8 the activity of SrLip was registered only when *p*-NPP is incorporated in Na-deoxycholate (Fig. 1c)) since only in this spectrum a new band (*p*-nitrophenolate) appears at 399 nm. Although a mixture of *p*-nitrophenolate and *p*-nitrophenol can be expected at pH around 7 [51], it seems that only the former appears in this system (Fig. 1c). In the presence of inactive SrLipSer10/A barely detected maxima at 403 nm and 416 nm suggested that *p*-nitrophenolate may be produced simply by hydrolysis and is found in slightly different immediate environment (Fig. 1c). Corresponding signature is not seen when *p*-NPP is incorporated in gum Arabic (Fig. 1a)) or DOPC liposomes for *x*(*p*-NPP) = 0 % (Fig. 1e)). However, for DOPC liposomes for *x*(*p*-NPP) = 2 % / 20 % (Fig. 1e)), respectively, there is some chance that *p*-nitrophenol (350 nm / 355 nm) and *p*-nitrophenolate ( − / 377 nm) is generated (as the quantification of SrLip activity is not the focus of this work, their ratios were not further investigated). Further, the position of exceptionally broad signal with maximum at 377 nm for *x*(*p*-NPP) = 20 % in the presence of SrLip may be related with the impact of the surface structural and charge distribution properties on *p*-nitrophenolate (the *-labelled spectra are upscaled by 0.45 in order to improve their visibility).

In a medium of pH value 10.0 very weak signals at 387 nm in the presence of SrLipSer10/A and at 409 nm in the presence of SrLip are most likely the result of *p*-NPP hydrolysis embedded in

gum Arabic (Fig. 1b) in slightly different surroundings rather than lipases catalytic activity. In addition, the extremely low absorbance of the signal, together with the accompanying noise, suggests a very low concentration of the resulting species (Fig. 1b)). When *p*-NPP is incorporated in Na-deoxycholate at pH = 10.0 a signature of *p*-nitrophenolate appears a 406 nm in the presence of SrLip, whereas the presence of inactive mutant SrLipSer10/A, as expected, hardly causes a rise from the baseline (Fig. 1d)). As for the impact of DOPC is concerned, the formation of *p*-nitrophenolate is suggested only for $x$(*p*-NPP) = 20 % (the *-labelled spectra are upscaled by 0.1 ($x$(*p*-NPP) = 2 %) and 0.3 ($x$(*p*-NPP) = 20 %) in order to enhance their visibility); in particular, a broad and distinct signal with maximum at 390 nm in the presence of SrLip suggest that *p*-NPP might achieve an orientation and distribution favorable for SrLip to manifest its catalytic activity. The importance of this finding lies in the fact that so far, at best of our knowledge, it has been shown that the negatively charged surface is a key factor for the interfacial activation of different lipases to occur [32]. The observed phenomenon clearly indicates that even the zwitterionic surface (DOPC), with a certain orientation and way of substrate ordering, might enable the interfacial activation. Finally, a very weak signal at 378 nm in the presence of SrLipS10/A (Fig. 1f) probably originates due to *p*-NPP hydrolysis (additionally, carbonate-bicarbonate buffer might contribute to the activity enhancement [52]). As far as the lack of corresponding signal in a mixture of gum Arabic and *p*-NPP is concerned, it is very likely that *p*-NPP is hidden from the surface so lipase can not get in touch with it (more thorough description related with this assumption is presented in when MD results are discussed).

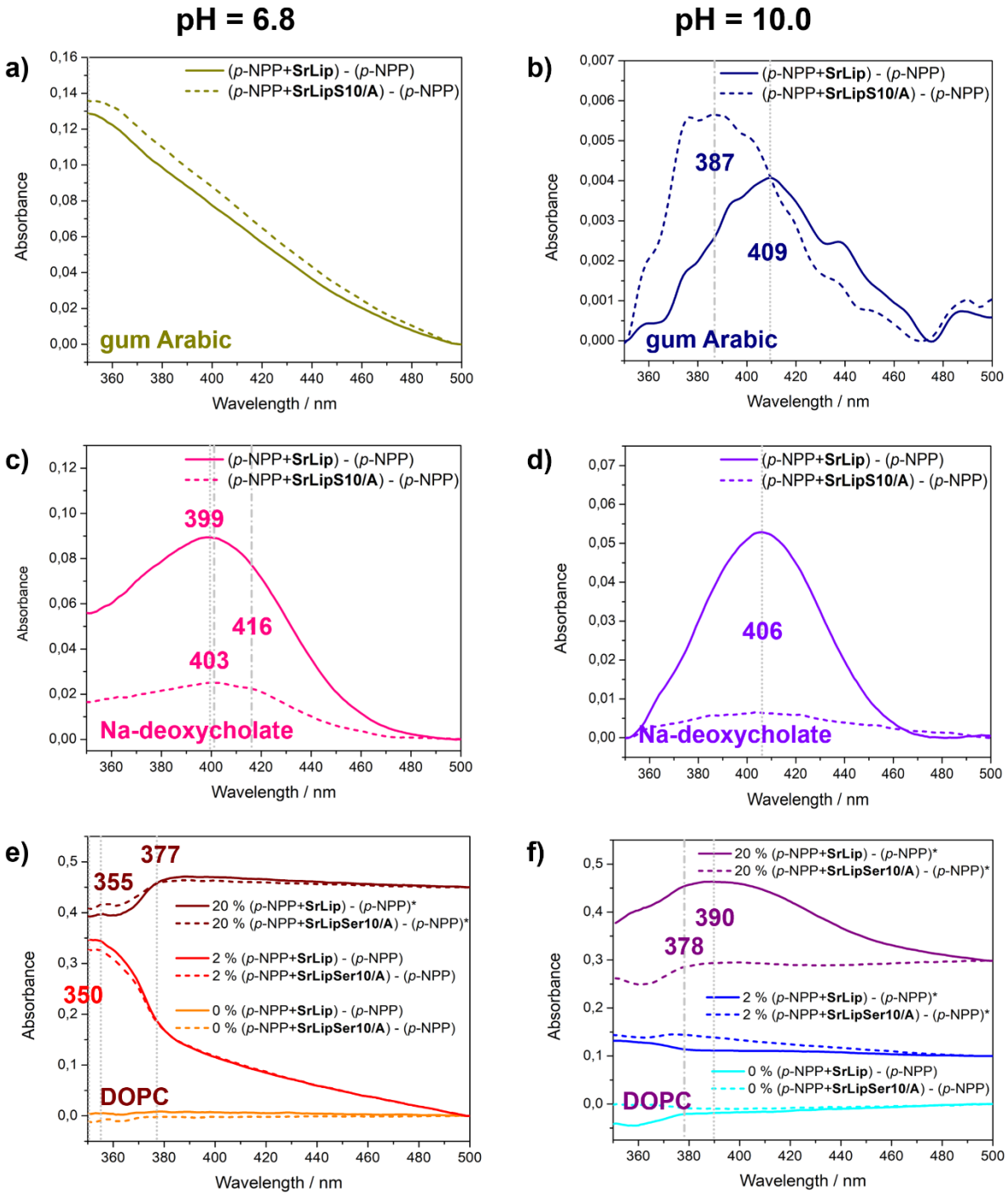


Fig. 1. Subtracted UV/Vis spectra of *p*-NPP in the presence of SrLip (solid curves) and SrLip S10/A (short dashed curves) when found in chemically different surroundings at two pH values (6.8 left column and 10.0 right column): in gum Arabic (a) dark yellow curves and b) navy curves), in Na-deoxycholate (c) pink curves and d) violet curves), and in DOPC liposomes (e)

orange ($x$($p$-NPP) = 0 %), red ($x$($p$-NPP) = 2 %) and wine ($x$($p$-NPP) = 20 %) curves and f) cyan ($x$($p$-NPP) = 0 %), blue ($x$($p$-NPP) = 2 %) and purple ($x$($p$-NPP) = 20 %) curves). The *-labelled spectra are upscaled in order to improve their visibility.

In order to provide more thorough characterization of the $p$-NPP arrangment in DOPC lipid bilayers, we examined phase behavior of DPPC with incorporated $p$-NPP by DSC (Fig. 2).

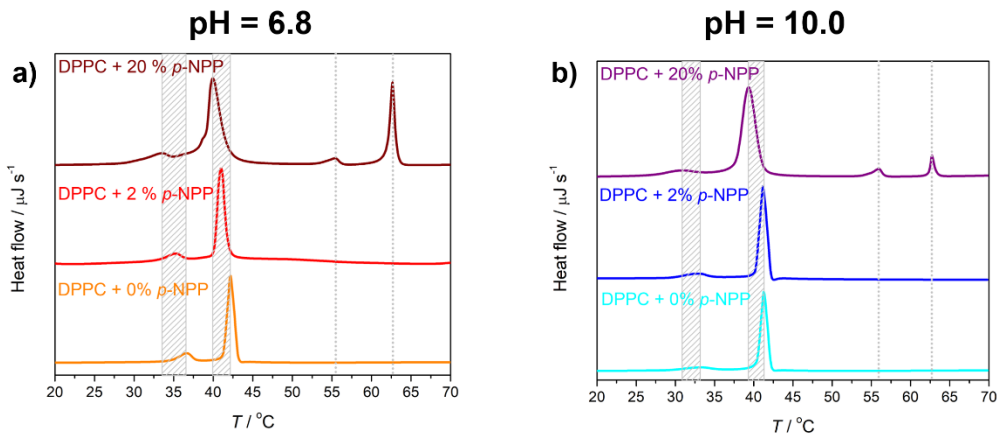


Fig. 2. DSC curves of liposomes constituted from DPPC lipids suspended in buffers of two pH values (6.8 and 10.0) with $x$($p$-NPP) = 0 % (orange curve for pH 6.8 (a) and cyan curve for pH 10.0 (b)), 2 % (red curve for pH 6.8 (a) and blue curve for pH 10.0 (b)), 20 % (wine curve for pH 6.8 (a) and purple curve for pH 10.0 (b)).

In the absence of $p$-NPP measured $T_p$ and $T_m$ of DPPC are found at 36.5 °C and 42.2 °C in suspension of pH = 6.8 and at 33.4 °C and 41.3 °C at pH = 10.0, respectively (Table 1). Their mutual differences are attributed to the change in pH value of a medium and are in satisfactorily agreement with reported values [53,54]. In the presence of $p$-NPP the appearance of DSC curve changes differently depending on the amount of incorporated $p$-NPP; at mole ratio $x$($p$-NPP) = 2 % induces small shift of both phase transitions to lower temperatures and still keeps them separate (Table 1), whereas for $x$($p$-NPP) = 20 % $T_p$ is shifted for about 3 °C and $T_m$ for 2-3 °C in comparison with suspensions of pure DPPC, regardless of the pH value (Table 1). Two additional phase transitions (labelled as $T_x$ and $T_y$ in Table 1) are observed at ~ 56 °C and ~ 63 °C (Table 1) in both suspensions and are assigned to the melting of PA in micellar and crystalline form, respectively [54,55], formed due to presumably temperature-induced hydrolysis of $p$-NPP [56] regardless of the pH of the solutions [57].

Table 1. Phase transition temperatures of DPPC lipids suspended in buffers of two pH values (6.8 and 10.0) with *x*(*p*-NPP) = 0 %, 2 % and 20 %.

| *x*(*p*-NPP) in DPPC | pH = 6.8 | | | | pH = 10.0 | | | |
|---|---|---|---|---|---|---|---|---|
| | $T_p$ [a] | $T_m$ [a] | $T_x$ [a] | $T_y$ [a] | $T_p$ [a] | $T_m$ [a] | $T_x$ [a] | $T_y$ [a] |
| 0 % | 36.5 | 42.2 | – | – | 33.3 | 41.3 | – | – |
| 2 % | 35.1 | 41.2 | – | – | 32.9 | 41.1 | – | – |
| 20 % | 33.5 | 39.9 | 55.5 | 62.7 | 30.8 | 39.3 | 55.9 | 62.8 |

[a] In °C. Uncertainty associated with particular phase transition temperature determined from curve maximum is ± 0.1 °C.

As DSC curve remains effectively unchanged for pure DPPC and for DPPC with *x*(*p*-NPP) = 2 %, *p*-NPP molecules are very likely statistically distributed over the lipid bilayer. For *x*(*p*-NPP) = 20 % it might be that, due to the temperature-induced hydrolysis of *x*(*p*-NPP), some PA molecules remain embedded in DPPC bilayer, whereas certain portion of them forms phase separated domains that crystallize and micelles as structurally different supramolecular aggregates [58].

Possible differences in the behavior of *p*-NPP with respect to different environments are unraveled using MD simulations. More precisely, we are particularly interested in the possible differences in positioning of *p*-NPP inside the respective biological/organic layers, namely model gum Arabic, Na-deoxycholate and DOPC (bi)layers. In this respect, number density profiles of *p*-NPP, water and the main bilayer/layer constituent X (X denotes model gum Arabic, Na-deoxycholate and DOPC) are calculated and shown in Fig. 3, while single snapshots of the three investigated systems taken at the very end of 150 ns MD simulations are given in the Fig. 3.

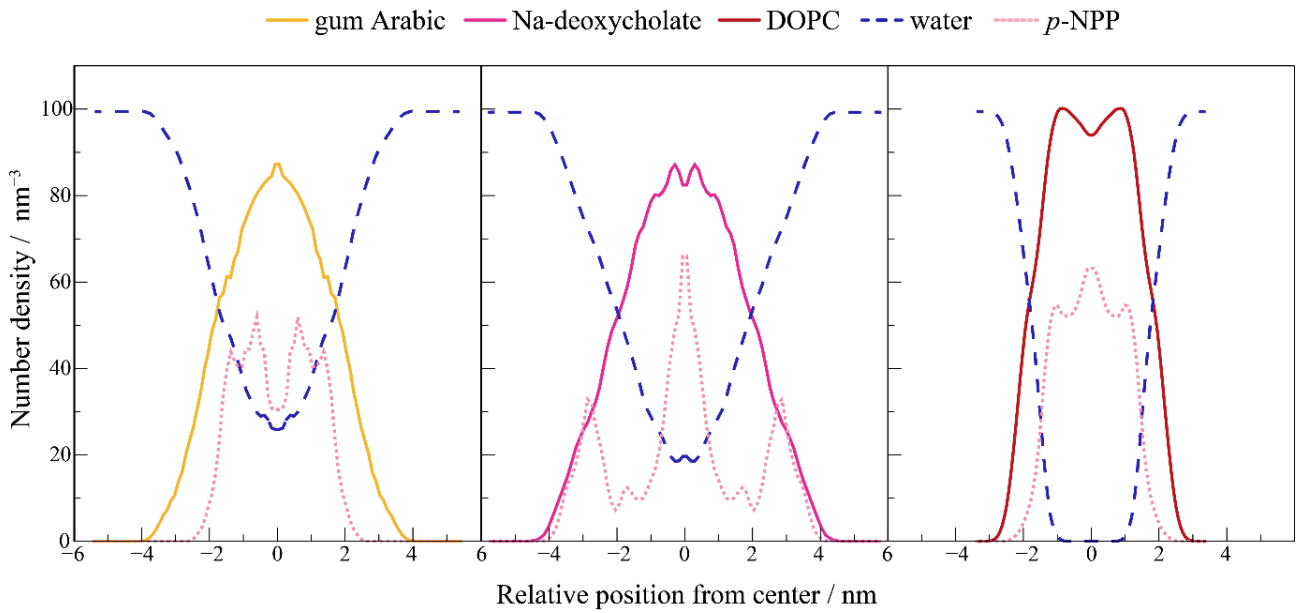


Fig. 3. Symmetrized number density profiles along the direction perpendicular to the layers (z-direction) of the main system constituents for all three simulated systems. Left panel: model gum Arabic system. Middle panel: Na-deoxycholate system. Right panel: DOPC system. Number density of *p*-NPP was scaled for comparison purposes (*p*-NPP constitutes only 5-10% of the respective layers, thus its number density is significantly smaller compared to the present main constituent/water number density).

Inspection of the obtained number density profiles shows drastic differences in both the overall and *p*-NPP specific behavior of the investigated systems. More precisely, we can easily observe that only DOPC bilayer is virtually impenetrable with respect to water molecules, while both layers containing Na-deoxycholate and model gum Arabic moieties contain rather significant amount of water molecules even in the very center of their respective layers (compare blue dashed lines in Fig. 3). This is naturally expected, as only DOPC bilayer possesses strong hydrophobic character in its central region (both Na-deoxycholate and model gum Arabic layers contain significant amounts of hydrophilic groups, which are present to certain extent in all regions of their respective layers). More importantly, we observe rather marked differences in the behavior of *p*-NPP in the three simulated scenarios. In this regard, we firstly observe that *p*-NPP tends to reside in two different regions in the deoxycholate layer, possessing peaks at the center of the deoxycholate layer and at the very deoxycholate/water interface (Fig. 3, middle panel), which makes this layer drastically different compared to either model gum Arabic or

DOPC layers, in which *p*-NPP tends to exclusively reside inside the present (bi)layers. Secondly, even though *p*-NPP tends to reside inside the model gum Arabic and DOPC layers, closer comparison of the two reveals that, on average, it resides more deeply buried inside the model gum Arabic layer. In this respect, *p*-NPP is more readily turned toward DOPC/water interface with its head group (4-nitrophenol group) compared to the situation in the model gum Arabic layer, in which *p*-NPP is significantly more randomly oriented with respect to the present organic/water interface (compare left and right images in Fig. 4). We thus find that, with respect to the availability of *p*-NPP molecules at the very water interfaces of the three systems, that Na-deoxycholate > DOPC > model gum Arabic, correlating perfectly with the performed experiments, showing that the activity is by far most pronounced in the case of Na-deoxycholate (Fig. 4, middle image), followed by DOPC and gum Arabic systems.

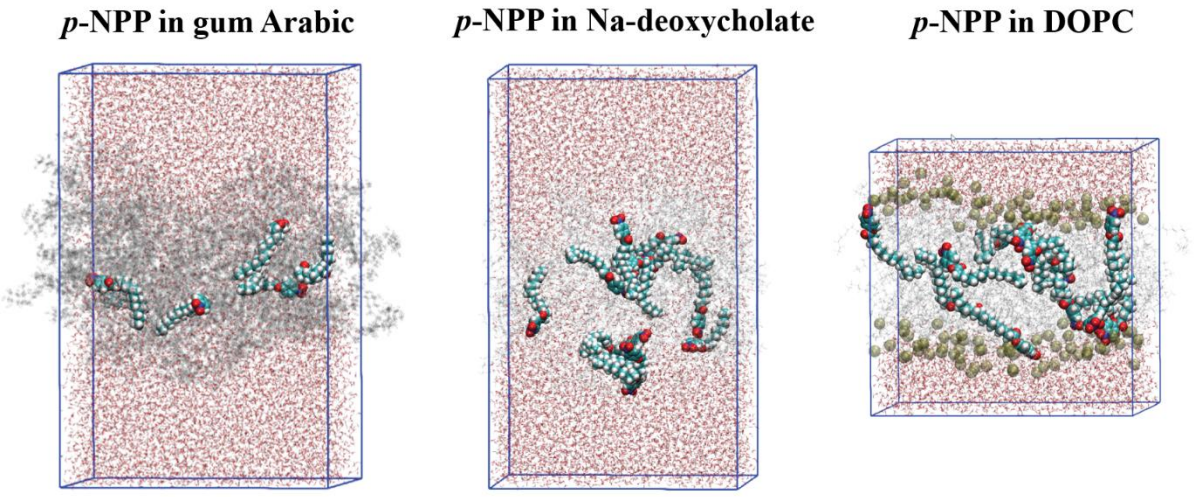


Fig. 4. Snapshots of the three systems at the very end of their respective 150 ns long MD simulations. a) model gum Arabic, b) Na-deoxycholate and c) DOPC systems. Water molecules are shown in translucent representation, model gum Arabic, deoxycholate and DOPC lipids are shown in the ghost mode (light gray color), phosphate atoms belonging to lipid heads are shown in translucent yellow spherical representation, with *p*-NPP molecules being shown using spherical representation (vdW representation, carbon atoms in cyan, hydrogen atoms in white, oxygen atoms in red, and nitrogen atoms in blue color).

It is also worth noting that different aggregation of *p*-NPP molecules is observed in the three simulated scenarios, with aggregation being most strongly observed in Na-deoxycholate,

followed closely by DOPC, finally being virtually unobserved in the model gum Arabic layer (see Fig. S6), which could also be an important factor in the overall activity, as measured via experiments.

Lastly, we investigate the specific interactions that *p*-NPP molecules form with the main constituents of the respective (bi)layers in which they were incorporated. In this respect, we calculated the average number of hydrogen bonds (HBs) formed between a single *p*-NPP moiety (average over last 50 ns and over all present *p*-NPP molecules) and either present water molecules or hydrogen donor groups found in the main constituents (model gum Arabic, Na-deoxycholate and DOPC). Interestingly, we find that single *p*-NPP molecule, via its head group, forms 2.7 HBs in the model gum Arabic system, 1.7 HBs in Na-deoxycholate, and only 1.0 HB in DOPC, on average (see Table 2 for details, DOPC cannot form HBs with *p*-NPP as it contains only hydrogen bond acceptors, i.e., no HB acceptor-donor pairs available). This finding thus partially explains the trends observed in number density profiles presented in Fig. 3. More precisely, due to the fact that *p*-NPP forms > 1 HBs on average more in the case of model gum Arabic system than it forms in both Na-deoxycholate and DOPC systems, it is rather expected that the head group of *p*-NPP is significantly more stabilized in the center of the model gum Arabic layer compared to the same group when considering either Na-deoxycholate or DOPC (bi)layers. Thus, one can expect significantly larger energetic penalty when going from central towards interfacial region in the case of *p*-NPP molecules in the model gum Arabic system compared to the two remaining model environments.

Table 2. Average number of hydrogen bonds and corresponding standard deviation between a single *p*-NPP molecule and water molecules, and between a single *p*-NPP molecule and compounds X, with X representing the main (bi)layer constituents, i.e., model gum Arabic, Na-deoxycholate and DOPC.

| Self-assembled aggregate (X) | Averagen number of HBs | |
|---|---|---|
| | *p*-NPP ··· water | *p*-NPP ··· X |
| Gum Arabic | 1.8 ± 0.4 | 0.9 ± 0.3 |
| Na-deoxycholate | 1.2 ± 0.2 | 0.5 ± 0.1 |
| DOPC | 1.0 ± 0.3 | – |

Finally, the obtained experimental and computational data clearly show that for interfacial activation of lipase the key is the coupling between the surface charge of emulsifier (gum Arabic or Na-deoxycolate) or matrix in which *p*-NPP (DOPC) molecules and (local) concentrations or arrangements are embedded. If only one of these two conditions is met, interfacial activation is absent. To the best of our knowledge, this manuscript presents a unique experimental and computational study that has deciphered which combination of specific factors is essential for interfacial activation of *Streptomyces rimosus* lipase [22,59] .

## 5. Conclusion

In this manuscript we examined the catalytic activity of SrLip (in comparison with an inactive mutant SrLipS10/A) towards *p*-NPP in order to unravel which conditions have to be met to get to the interfacial activation. With this respect, *p*-NPP was anchored at three different interfaces for the first time: gum Arabic, Na-deoxycholate and DOPC liposomes, that differ in surface charge and substrate accommodation in terms of its position and orientation. Additionally, the concentration of *p*-NPP incorporated in DOPC liposomes varied so that SrLip catalytic activity as a function of substrate concentration/arrangement only was examined as well. Spectrophotometric results demonstrated that SrLip catalyses hydrolysis of an ester bond of *p*-NPP significantly when the latter is embedded in Na-deoxycholate, regardless to the pH value, suggesting that the combination of a favorable surface charge and substrate position dictates the occurrence of interfacial activation. When *p*-NPP was incorporated in liposomes constituted from zwitterionic DOPC the activity was the strongest for $x$(*p*-NPP) = 20 %, suggesting that surface features combined with substrate orientation and arrangement may provide the conditions for the interfacial activation to occur [32]. Molecular picture of *p*-NPP at particular interface provided from MD simulations confirmed that the availability of the substrate is the greatest when embedded in Na-deoxycholate and the smallest in model gum Arabic, respectively.

## Acknowledgment

This paper was supported by the Croatian Science Foundation, Project Nos. UIP-2020-02-7669, IP-2018-01-1754 and IP-2018-01-5475. The authors gratefully acknowledge Dr. Darija Domazet

Jurašin and Dr. Maja Dutour Sikirić (Laboratory for biocolloids and surface chemistry, Ruđer Bošković Institute) for making DLS measurements and for a support in optical microscopy. The authors sincerely thank the reviewers (especially referee #1) for their helpful advice and comments, which, in our humble opinion, significantly improved the manuscript.

**Supporting Information**

Supporting Information associated with this paper can be found in the online version at http://.

**References:**

[1] Macrae, A. R.; Hammond, R. C. Present and Future Applications of Lipases. *Biotechnol. Genet. Eng. Rev.* **1985**, *3* (1), 193–217. https://doi.org/10.1080/02648725.1985.10647813.

[2] Abramić, M.; Leščić, I.; Korica, T.; Vitale, L.; Saenger, W.; Pigac, J. Purification and Properties of Extracellular Lipase from *Streptomyces Rimosus*. *Enzyme Microb. Technol.* **1999**, *25*, 522–529.

[3] Khan, F. I.; Lan, D.; Durrani, R.; Huan, W.; Zhao, Z.; Wang, Y. The Lid Domain in Lipases: Structural and Functional Determinant of Enzymatic Properties. *Front. Bioeng. Biotechnol.* **2017**, *5* (MAR), 1–13. https://doi.org/10.3389/fbioe.2017.00016.

[4] Gupta, R.; Gupta, N.; Rathi, P. Bacterial Lipases: An Overview of Production, Purification and Biochemical Properties. *Appl. Microbiol. Biotechnol.* **2004**, *64* (6), 763–781. https://doi.org/10.1007/s00253-004-1568-8..

[5] Ramnath, L.; Sithole, B.; Govinden, R. Classification of Lipolytic Enzymes and Their Biotechnological Applications in the Pulping Industry. *Can. J. Microbiol.* **2017**, *63* (3), 179–192. https://doi.org/10.1139/cjm-2016-0447.

[6] Arpigny, J. L.; Jaeger, K. E. Bacterial Lipolytic Enzymes: Classification and Properties. *Biochem. J.* **1999**, *343* (1), 177–183. https://doi.org/10.1042/0264-6021:3430177.

[7] Biđin, S.; Vujaklija, I.; Paradžik, T.; Bielen, A.; Vujaklija, D. Leitmotif: Protein Motif Scanning 2.0. *Bioinformatics* **2020**, *36* (11), 2566–3567.

[8] Su, H. G.; Zhang, X. H.; Wang, T. T.; Wei, W. L.; Wang, Y. X.; Chen, J.; Zhou, Y. Bin;

Chen, M.; Ma, Y. Z.; Xu, Z. S.; Min, D. H. Genome-Wide Identification, Evolution, and Expression of GDSL-Type Esterase/Lipase Gene Family in Soybean. *Front. Plant Sci.* **2020**, *11* (June), 726, 19. https://doi.org/10.3389/fpls.2020.00726.

[9] Vujaklija, D.; Schröder, W.; Abramić, M.; Zou, P.; Leščić, I.; Franke, P.; Pigac, J. A Novel Streptomycete Lipase: Cloning, Sequencing and High-Level Expression of the *Streptomyces Rimosus* GDS(L)-Lipase Gene. *Arch. Microbiol.* **2002**, *178* (2), 124–130. https://doi.org/10.1007/s00203-002-0430-6.

[10] I Vujaklija, I.; Bielen, A.; Paradžik, T.; Bidin, S.; Goldstein, P.; Vujaklija, D. An Effective Approach for Annotation of Protein Families with Low Sequence Similarity and Conserved Motifs: Identifying GDSL Hydrolases across the Plant Kingdom. *BMC Bioinformatics* **2016**, *17*, 91, 17. https://doi.org/10.1186/s12859-016-0919-7

[11] Vujaklija, D.; Abramić, M.; Leščić, I.; Maršić, T.; Pigac, J. *Streptomyces Rimosus* GDS(L) Lipase: Production, Heterologous Overexpression and Structure-Stability Relationship. *Food Technol. Biotechnol.* **2003**, *41* (1), 89–93..

[12] Zehl, M.; Leščić, I.; Abramíc, M.; Rizzi, A.; Kojić-Prodić, B.; Allmaier, G. Characterization of Covalently Inhibited Extracellular Lipase from *Streptomyces Rimosus* by Matrix-Assisted Laser Desorption/Ionization Time-of-Flight and Matrix-Assisted Laser Desorption/Ionization Quadrupole Ion Trap Reflectron Time-of-Flight Mass Spectr. *J. Mass Spectrom.* **2004**, *39* (12), 1474–1483. https://doi.org/10.1002/jms.750.

[13] Leščić Ašler, I.; Zehl, M.; Kovačić, F.; Müller, R.; Abramić, M.; Allmaier, G.; Kojić-Prodić, B. Mass Spectrometric Evidence of Covalently-Bound Tetrahydrolipstatin at the Catalytic Serine of *Streptomyces Rimosus* Lipase. *Biochimica et Biophysica Acta - General Subjects*. 2007, pp 163–170. https://doi.org/10.1016/j.bbagen.2006.10.011.

[14] Leščić Ašler, I.; Štefanić, Z.; Maršavelski, A.; Vianello, R.; Kojić-Prodić, B. Catalytic Dyad in the SGNH Hydrolase Superfamily: In-Depth Insight into Structural Parameters Tuning the Catalytic Process of Extracellular Lipase from *Streptomyces Rimosus*. *ACS Chem. Biol.* **2017**, *12*, 1928–1936. https://doi.org/https://pubs.acs.org/doi/10.1021/acschembio.6b01140.

[15] Louwrier, A.; Drtina, G. J.; Klibanov, A. M. On the Issue of Interfacial Activation of Lipase in Nonaqueous Media. *Biotechnol. Bioeng.* **1996**, *50* (1), 1–5. https://doi.org/10.1002/(SICI)1097-0290(19960405)50:1<1::AID-BIT1>3.0.CO;2-L.

[16] Verger, R. "Interfacial Activation" of Lipases: Facts and Artifacts. *Trends Biotechnol.* **1997**, *15* (1), 32–38. https://doi.org/10.1016/S0167-7799(96)10064-0.

[17] Brzozowski, A. M.; Derewenda, U.; Derewenda, Z. S.; Dodson, G. G.; Lawson, D. M.; Turkenburg, J. P.; Bjorkling, F.; Huge-Jensen, B.; Patkar, S. A.; Thim, L. A Model for Interfacial Activation in Lipases from the Structure of a Fungal Lipase-Inhibitor Complex. *Nature*. 1991, pp 491–494. https://doi.org/10.1038/351491a0..

[18] Mala, J. G. S.; Takeuchi, S. Understanding Structural Features of Microbial Lipases - An Overview. *Anal. Chem. Insights* **2008**, *2008* (3), 9–19. https://doi.org/10.4137/aci.s551.

[19] Adlercreutz, P. Immobilisation and Application of Lipases in Organic Media. *Chem. Soc. Rev.* **2013**, *42* (15), 6406–6436. https://doi.org/10.1039/c3cs35446f.

[20] Leščić, I.; Vukelić, B.; Majerić-Elenkov, M.; Saenger, W.; Abramić, M. Substrate Specificity and Effects of Water-Miscible Solvents on the Activity and Stability of Extracellular Lipase from *Streptomyces Rimosus*. *Enzyme Microb. Technol.* **2001**, *29*, 548–553.

[21] Wickham, M.; Garrood, M.; Leney, J.; Wilson, P. D. G.; Fillery-Travis, A. Modification of a Phospholipid Stabilized Emulsion Interface by Bile Salt: Effect on Pancreatic Lipase Activity. *J. Lipid Res.* **1998**, *39* (3), 623–632. https://doi.org/10.1016/s0022-2275(20)33300-9.

[22] Reis, P.; Holmberg, K.; Watzke, H.; Leser, M. E.; Miller, R. Lipases at Interfaces: A Review. *Adv. Colloid Interface Sci.* **2009**, *147–148* (C), 237–250. https://doi.org/10.1016/j.cis.2008.06.001.

[23] Skjold-Jørgensen, J.; Vind, J.; Svendsen, A.; Bjerrum, M. J. Altering the Activation Mechanism in *Thermomyces Lanuginosus* Lipase. *Biochemistry* **2014**, *53* (25), 4152–4160. https://doi.org/10.1021/bi500233h

[24] Burdette, R. A.; Quinn, D. M. Interfacial Reaction Dynamics and Acyl-Enzyme Mechanism for Lipoprotein Lipase-Catalyzed Hydrolysis of Lipid *p*-Nitrophenyl Esters. *J. Biol. Chem.* **1986**, *261* (26), 12016–12021. https://doi.org/10.1016/s0021-9258(18)67195-9.

[25] Sanchez, C.; Schmitt, C.; Kolodziejczyk, E.; Lapp, A.; Gaillard, C.; Renard, D. The Acacia Gum Arabinogalactan Fraction Is a Thin Oblate Ellipsoid: A New Model Based on Small-Angle Neutron Scattering and *Ab Initio* Calculation. *Biophys. J.* **2008**, *94* (2), 629–639. https://doi.org/10.1529/biophysj.107.109124

[26] Tiss, A.; Carrière, F.; Verger, R. Effects of Gum Arabic on Lipase Interfacial Binding and Activity. *Anal. Biochem.* **2001**, *294* (1), 36–43. https://doi.org/10.1006/abio.2001.5095.

[27] Sethuraman, S.; Rajendran, K. Is Gum Arabic a Good Emulsifier Due to CH...π Interactions? How Urea Effectively Destabilizes the Hydrophobic CH...π Interactions in the Proteins of Gum Arabic than Amides and GuHCl? *ACS Omega* **2019**, *4* (15), 16418–16428. https://doi.org/10.1021/acsomega.9b01980

[28] Rabelo, R. S.; Tavares, G. M.; Prata, A. S.; Hubinger, M. D. Complexation of Chitosan with Gum Arabic, Sodium Alginate and κ-Carrageenan: Effects of pH, Polymer Ratio and Salt Concentration. *Carbohydr. Polym.* **2019**, *223* (July), 115120. https://doi.org/10.1016/j.carbpol.2019.115120.

[29] Bielen, A.; Ćetković, H.; Long, P. F.; Schwab, H.; Abramić, M.; Vujaklija, D. The SGNH-Hydrolase of *Streptomyces Coelicolor* Has (Aryl)Esterase and a True Lipase Activity. *Biochimie* **2009**, *91* (3), 390–400. https://doi.org/10.1016/j.biochi.2008.10.018.

[30] Lazzari, F.; Alexander, B. D.; Dalgliesh, R. M.; Alongi, J.; Ranucci, E.; Ferruti, P.; Griffiths, P. C. pH-Dependent Chiral Recognition of D- and L-Arginine Derived Polyamidoamino Acids by Self-Assembled Sodium Deoxycholate. *Polymers (Basel).* **2020**, *12* (4), 900, 15. https://doi.org/10.3390/POLYM12040900..

[31] Cajal, Y.; Svendsen, A.; Girona, V.; Patkar, S. A.; Alsina, M. A. Interfacial Control of Lid Opening in *Thermomyces Lanuginosa* Lipase. *Biochemistry* **2000**, *39* (2), 413–423. https://doi.org/10.1021/bi991927i.

[32] Bohr, S. S. R.; Thorlaksen, C.; Kühnel, R. M.; Günther-Pomorski, T.; Hatzakis, N. S. Label-Free Fluorescence Quantification of Hydrolytic Enzyme Activity on Native Substrates Reveals How Lipase Function Depends on Membrane Curvature. *Langmuir* **2020**, *36* (23), 6473–6481. https://doi.org/10.1021/acs.langmuir.0c00787.

[33] Koynova, R.; Caffrey, M. Phases and Phase Transitions of the Phosphatidylcholines. *Biochim. Biophys. Acta* **1998**, *1376*, 91–145. https://doi.org/10.1016/S0013-4686(03)00208-1.

[34] DeSanti, C. L.; Strohl, W. R. Characterization of the *Streptomyces* Sp. Strain C5 Snp Locus and Development of Snp-Derived Expression Vectors. *Appl. Environ. Microbiol.* **2003**, *69* (3), 1647–1654. https://doi.org/10.1128/AEM.69.3.1647-1654.2003.

[35] Filić, Ž.; Bielen, A.; Ćehić, M.; Šarić, E.; Crnolatac, I.; Tomić, S.; Abramić, M.; Vujaklija, D. *Manuscript in Preparation.*, **27.10.2022.**

[36] Xia, Y.; Xu, C.; Zhang, X.; Ning, P.; Wang, Z.; Tian, J.; Chen, X. Liposome-Based Probes for Molecular Imaging: From Basic Research to the Bedside. *Nanoscale* **2019**, *11* (13), 5822–5838. https://doi.org/10.1039/C9NR00207C.

[37] Menges, F. "Spectragryph - optical spectroscopy software", Version 1.2.15, 2015, http://www.effemm2.de/spectragryph/ **25.10.2022.**

[38] Maleš, P.; Brkljača, Z.; Crnolatac, I.; Bakarić, D. Application of MCR-ALS with EFA on FT-IR Spectra of Lipid Bilayers in the Assessment of Phase Transition Temperatures: Potential for Discernment of Coupled Events. *Colloids Surfaces B Biointerfaces* **2021**, *201* (January), 111645, 8. https://doi.org/10.1016/j.colsurfb.2021.111645..

[39] Kondo, T.; Kichijo, M.; Maruta, A.; Nakaya, M.; Takenaka, S.; Arakawa, T.; Fushinobu, S.; Sakamoto, T. Structural and Functional Analysis of Gum Arabic L-Rhamnose-α-1,4-D-Glucuronate Lyase Establishes a Novel Polysaccharide Lyase Family. *J. Biol. Chem.* **2021**, *297* (3), 101001. https://doi.org/10.1016/j.jbc.2021.101001.

[40] Martínez, L.; Andrade, R.; Birgin, E. G.; Martínez, J. M. Software News and Updates. Packmol: A Package for Building Initial Configurations for Molecular Dynamics

Simulations. *J. Comput. Chem.* **2009**, *30*, 2157–2164. https://doi.org/10.1002/jcc.

[41] Martínez, L.; Andrade, R.; Birgin, E. G.; Martínez, J. M. Software News and Updates. Packmol: A Package for Building Initial Configurations for Molecular Dynamics Simulations. *J. Comput. Chem.* **2009**, *30*, 2157–2164. https://doi.org/10.1002/jcc.

[42] Wang, J.; Wolf, R. M.; Caldwell, J. W.; Kollman, P. A.; Case, D. A. Development and Testing of a General Amber Force Field. *J. Comput. Chem.* **2004**, *25* (9), 1157–1174. https://doi.org/10.1002/jcc.20035.

[43] Kirschner, K. N.; Yongye, A. B.; Tschampel, S. M.; González-Outeiriño, J.; Daniels, C. R.; Foley, B. L.; Woods, R. J. GLYCAM06: A Generalizable Biomolecular Force Field. Carbohydrates. *J. Comput. Chem.* **2008**, *29*, 622–655. https://doi.org/10.1002/jcc.

[44] Joung, I. S.; Cheatham III, T. E. Determination of Alkali and Halide Monovalent Ion Parameters for Use in Explicitly Solvated Biomolecular Simulations. *J. Phys. Chem. B* **2008**, *112* (30), 9020–9041. https://doi.org/10.1021/jp8001614.

[45] Cieplak, P.; Cornell, W. D.; Bayly, C.; Kollman, P. A. Application of the Multimolecule and to Biopolymers: Charge Derivation for Multiconformational RESP Methodology DNA, RNA, and Proteins. *J. Comput. Chem.* **1995**, *16* (11), 1357–1377. https://doi.org/10.1016/S0422-9894(08)70043-6.

[46] Darden, T.; York, D.; Pedersen, L. Particle Mesh Ewald: An *N*log(*N*) Method for Ewald Sums in Large Systems. *J. Chem. Phys.* **1993**, *98* (12), 10089–10092. https://doi.org/10.1063/1.464397.

[47] Abraham, M. J.; Murtola, T.; Schulz, R.; Páll, S.; Smith, J. C.; Hess, B.; Lindah, E. Gromacs: High Performance Molecular Simulations through Multi-Level Parallelism from Laptops to Supercomputers. *SoftwareX* **2015**, *1–2*, 19–25. https://doi.org/10.1016/j.softx.2015.06.001.

[48] Humphrey, W.; Dalke, A.; Schulten, K. VMD: Visual Molecular Dynamics. *J. Mol. Graph.* **1996**, *14*, 33–38. https://doi.org/10.1016/j.carbon.2017.07.012.

[49] Pliego, J.; Mateos, J. C.; Rodriguez, J.; Valero, F.; Baeza, M.; Femat, R.; Camacho, R.;

Sandoval, G.; Herrera-López, E. J. Monitoring Lipase/Esterase Activity by Stopped Flow in a Sequential Injection Analysis System Using p-Nitrophenyl Butyrate. *Sensors (Switzerland)* **2015**, *15* (2), 2798–2811. https://doi.org/10.3390/s150202798.

[50] Malathi, S.; Ezhilarasu, T.; Abiraman, T.; Balasubramanian, S. One Pot Green Synthesis of Ag, Au and Au-Ag Alloy Nanoparticles Using Isonicotinic Acid Hydrazide and Starch. *Carbohydr. Polym.* **2014**, *111* (April 2017), 734–743. https://doi.org/10.1016/j.carbpol.2014.04.105.

[51] Peng, Y.; Fu, S.; Liu, H.; Lucia, L. A. Accurately Determining Esterase Activity via the Isosbestic Point of *p*-Nitrophenol. *BioResources* **2016**, *11* (4), 10099–10111. https://doi.org/10.15376/biores.11.4.10099-10111.

[52] Iizuka, K.; Higurashi, H.; Fujimoto, J.; Hayashi, Y.; Yamamoto, K.; Hiura, H. Purification of Human Pancreatic Lipase and the Influence of Bicarbonate on Lipase Activity. *Ann. Clin. Biochem.* **1991**, *28* (4), 373–378. https://doi.org/10.1177/000456329102800411.

[53] Schullery, S. E.; Seder, T. A.; Weinstein, D. A.; Bryant, D. A. Differential Thermal Analysis of Dipalmitoylphosphatidylcholine-Fatty Acid Mixturest. *Biochemistry* **1981**, *20*, 6818–6824.

[54] Mabrey, S.; Sturtevant, J. M. Incorporation of Saturated Fatty Acids into Phosphatidylcholine Bilayers. *Biochim. Biophys. Acta (BBA)/Lipids Lipid Metab.* **1977**, *486* (3), 444–450. https://doi.org/10.1016/0005-2760(77)90094-7.

[55] Sathivel, S.; Prinyawiwatkul, W.; Negulescu, I. I.; King, J. M. Determination of Melting Points, Specific Heat Capacity and Enthalpy of Catfish Visceral Oil During the Purification Process. *JAOCS, J. Am. Oil Chem. Soc.* **2008**, *85* (3), 291–296. https://doi.org/10.1007/s11746-007-1191-9. [56] Weng, J.; Zhang, X. Enzymatic Hydrolysis of P-Nitrophenyl Butyrate in Water-in-Ionic Liquid Microemulsion. *Ferroelectrics* **2018**, *528* (1), 122–130. https://doi.org/10.1080/00150193.2018.1449439.

[57] Zuidam, N. J.; Crommelin, D. J. A. Differential Scanning Calorimetric Analysis of Dipalmitoylphosphatidylcholine-Liposomes upon Hydrolysis. *Int. J. Pharm.* **1995**, *126* (1–2), 209–217. https://doi.org/10.1016/0378-5173(95)04129-X.

[58] Fameau, A. L.; Ventureira, J.; Novales, B.; Douliez, J. P. Foaming and Emulsifying Properties of Fatty Acids Neutralized by Tetrabutylammonium Hydroxide. *Colloids Surfaces A Physicochem. Eng. Asp.* **2012**, *403*, 87–95. https://doi.org/10.1016/j.colsurfa.2012.03.059.

[59] Willems, N.; Lelimousin, M.; Koldsø, H.; Sansom, M. S. P. Interfacial Activation of M37 Lipase: A Multi-Scale Simulation Study. *Biochim. Biophys. Acta - Biomembr.* **2017**, *1859* (3), 340–349. https://doi.org/10.1016/j.bbamem.2016.12.012.